


# Journal Club 008

## CUPID-Mo performance and prospects



# The CUPID-Mo experiment for neutrinoless double-beta decay: performance and prospects

E. Armengaud<sup>1</sup>, C. Augier<sup>2</sup>, A. S. Barabash<sup>3</sup>, F. Bellini<sup>4,5</sup>, G. Benato<sup>6</sup>, A. Benoît<sup>7</sup>, M. Beretta<sup>8,9</sup>, L. Bergé<sup>10</sup>, J. Billard<sup>2</sup>, Yu. A. Borovlev<sup>11</sup>, Ch. Bourgeois<sup>12</sup>, M. Briere<sup>12</sup>, V. B. Brudanin<sup>13</sup>, P. Camus<sup>7</sup>, L. Cardani<sup>5</sup>, N. Casali<sup>5</sup>, A. Cazes<sup>2</sup>, M. Chapellier<sup>10</sup>, F. Charlieux<sup>2</sup>, M. de Combarieu<sup>14</sup>, I. Dafinei<sup>5</sup>, F. A. Danevich<sup>15</sup>, M. De Jesus<sup>2</sup>, L. Dumoulin<sup>10</sup>, K. Eitel<sup>16</sup>, E. Elkhoury<sup>2</sup>, F. Ferri<sup>1</sup>, B. K. Fujikawa<sup>17</sup>, J. Gascon<sup>2</sup>, L. Gironi<sup>8,9</sup>, A. Giuliani<sup>10,18,a</sup> , V. D. Grigorieva<sup>11</sup>, M. Gros<sup>1</sup>, E. Guerard<sup>12</sup>, D. L. Helis<sup>1</sup>, H. Z. Huang<sup>19</sup>, R. Huang<sup>6</sup>, J. Johnston<sup>20</sup>, A. Juillard<sup>2</sup>, H. Khalife<sup>10</sup>, M. Kleifges<sup>21</sup>, V. V. Kobychew<sup>15</sup>, Yu. G. Kolomensky<sup>6,22</sup>, S. I. Konovalov<sup>3</sup>, A. Leder<sup>20</sup>, P. Loaiza<sup>12</sup>, L. Ma<sup>19</sup>, E. P. Makarov<sup>11</sup>, P. de Marcillac<sup>10</sup>, L. Marini<sup>6,17,23</sup>, S. Marnieros<sup>10</sup>, D. Misiak<sup>2</sup>, X. -F. Navick<sup>1</sup>, C. Nones<sup>1</sup>, V. Novati<sup>10</sup>, E. Olivieri<sup>10</sup>, J. L. Ouellet<sup>20</sup>, L. Pagnanini<sup>8,9</sup>, P. Pari<sup>14</sup>, L. Pattavina<sup>23,24</sup>, B. Paul<sup>1</sup>, M. Pavan<sup>8,9</sup>, H. Peng<sup>25</sup>, G. Pessina<sup>9</sup>, S. Pirro<sup>23</sup>, D. V. Poda<sup>10,15</sup>, O. G. Polischuk<sup>15</sup>, E. Previtali<sup>8,9</sup>, Th. Redon<sup>10</sup>, S. Rozov<sup>13</sup>, C. Rusconi<sup>26</sup>, V. Sanglard<sup>2</sup>, K. Schäffner<sup>23</sup>, B. Schmidt<sup>17</sup>, Y. Shen<sup>19</sup>, V. N. Shlegel<sup>11</sup>, B. Siebenborn<sup>16</sup>, V. Singh<sup>6</sup>, S. Sorbino<sup>4,5</sup>, C. Tomei<sup>5</sup>, V. I. Tretyak<sup>15</sup>, V. I. Umatov<sup>3</sup>, L. Vagneron<sup>2</sup>, M. Velázquez<sup>27</sup>, M. Weber<sup>21</sup>, B. Welliver<sup>17</sup>, L. Winslow<sup>20</sup>, M. Xue<sup>25</sup>, E. Yakushev<sup>13</sup>, A. S. Zolotarova<sup>10</sup>

Time		
2017 Fall	Detector construction	CSNSM, Orsay, France
2018 January	Installation in the EDELWEISS-III cryostat	Modane
2018 Summer	Commissioning I	Modane
2019 Winter	Commissioning II	Modane
2019 March	Physics run	Modane

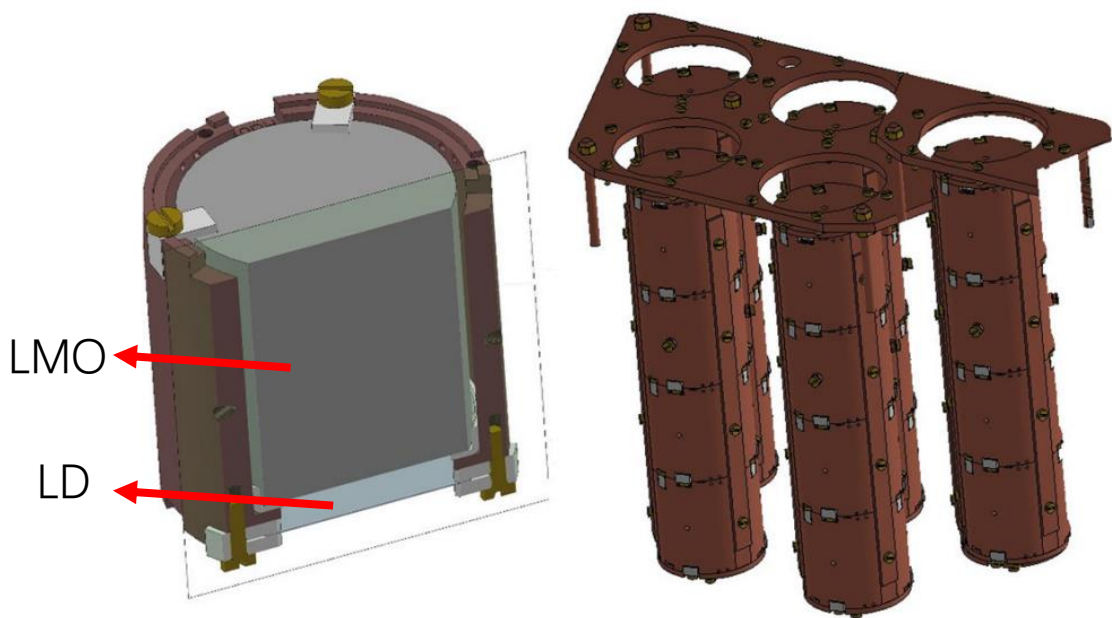
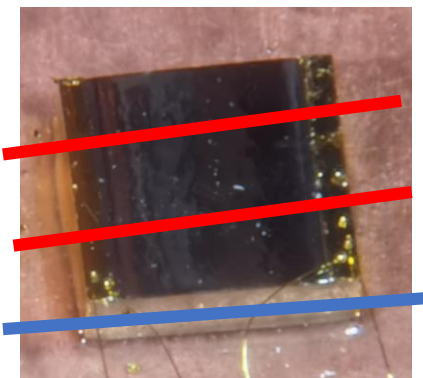
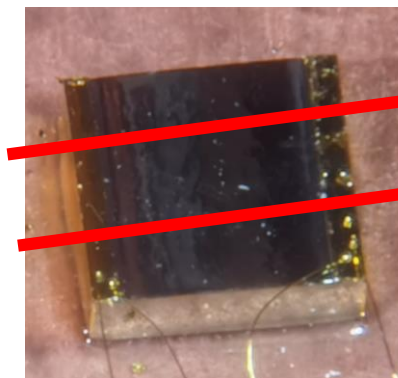


**Fig. 1** Rendering of a CUPID-Mo single detector module (left) designed to hold a  $\text{Li}_2^{100}\text{MoO}_4$  scintillating element. A module is comprised of a crystal of size  $\text{Ø}44 \times 45$  mm and a Ge wafer of  $\text{Ø}44 \times 0.175$  mm. The full 20-detector bolometric array is arranged in five suspended towers containing four detector modules each (right)

- 4 \* 5 array, LMO and LD at the bottom
- Czochralski technique; Radio-pure SiO powder slicing and surface treatment
- 44.5 mm \* 175  $\mu\text{m}$  Ge wafers, 70 nm SiO coated
- Dicing the NTDs for LDs to reduce their heat capacity



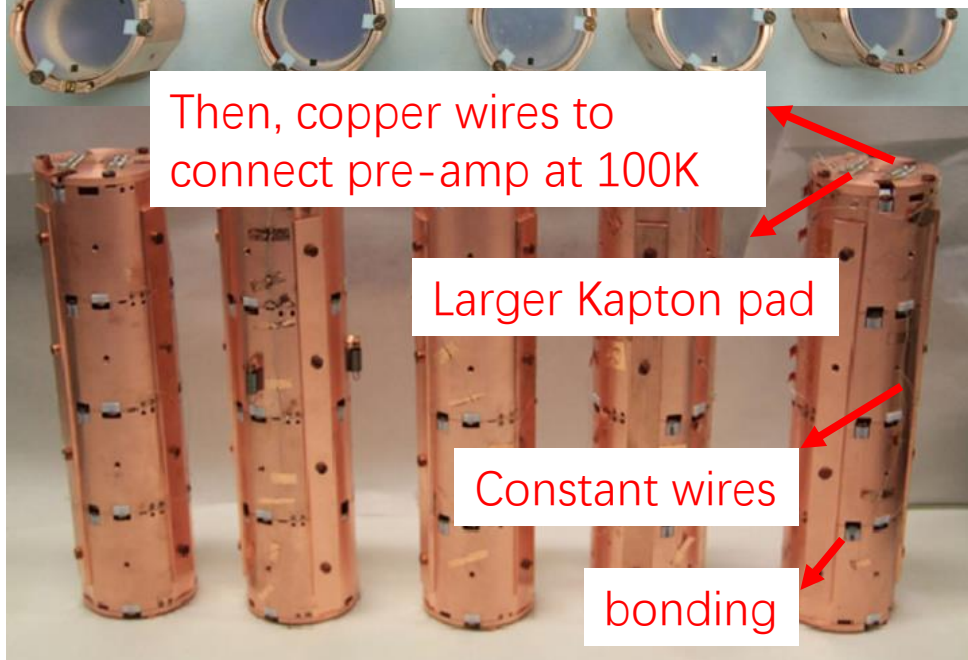
Commissioning I



Commissioning II



Fig. 4 An assembled CUPID-Mo module. On the left: view from the top, the semi-transparent crystal surface where the NTD and heater are located. On the right: view from the bottom, germanium LD with SiO coating (dark blue internal circle); the 2 mm on the edge of the wafer (17% of the area) are uncoated

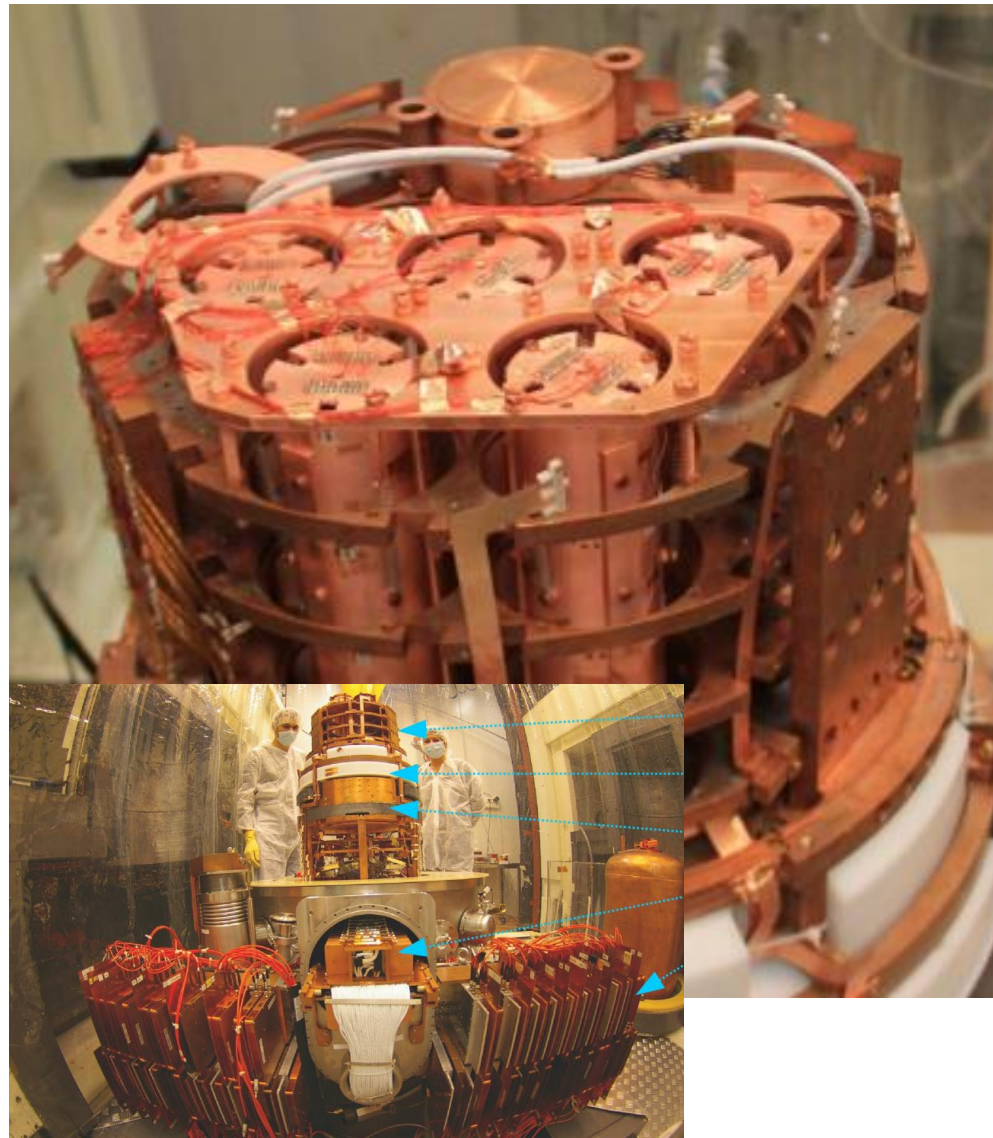


- No reflecting foil in Commissioning I; lateral side with reflecting foil (3M Vikuiti™) in Commissioning II
- Copper etched with citric acid, and PTFE in an ultrasonic bath with ethanol
- Tower assembly performed in a class 10 cleanroom

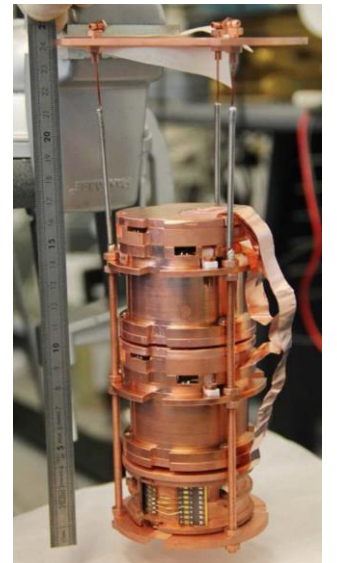
We bonded gold wires from the NTDs to flat Kapton pads with gold contacts to provide the electrical readout connection as well as the weak thermal link to the heat bath. In fact, the pads are glued on the copper detector holder, which is in excellent thermal contact with the coldest part of the dilution refrigerator. Silk-covered constantan twisted wires were sol-

dered on the other side of the pads and run up each tower to a larger Kapton pad with gold contacts glued at the top of the tower.

On this pad the constantan wires and copper wires (connection to the cold electronics) were soldered. This connection provides a link to Si-JFET (junction gate field-effect transistor) based pre-amplifiers at 100 K through the copper plate inside the EDELWEISS cryostat (see Sect. 2.8).

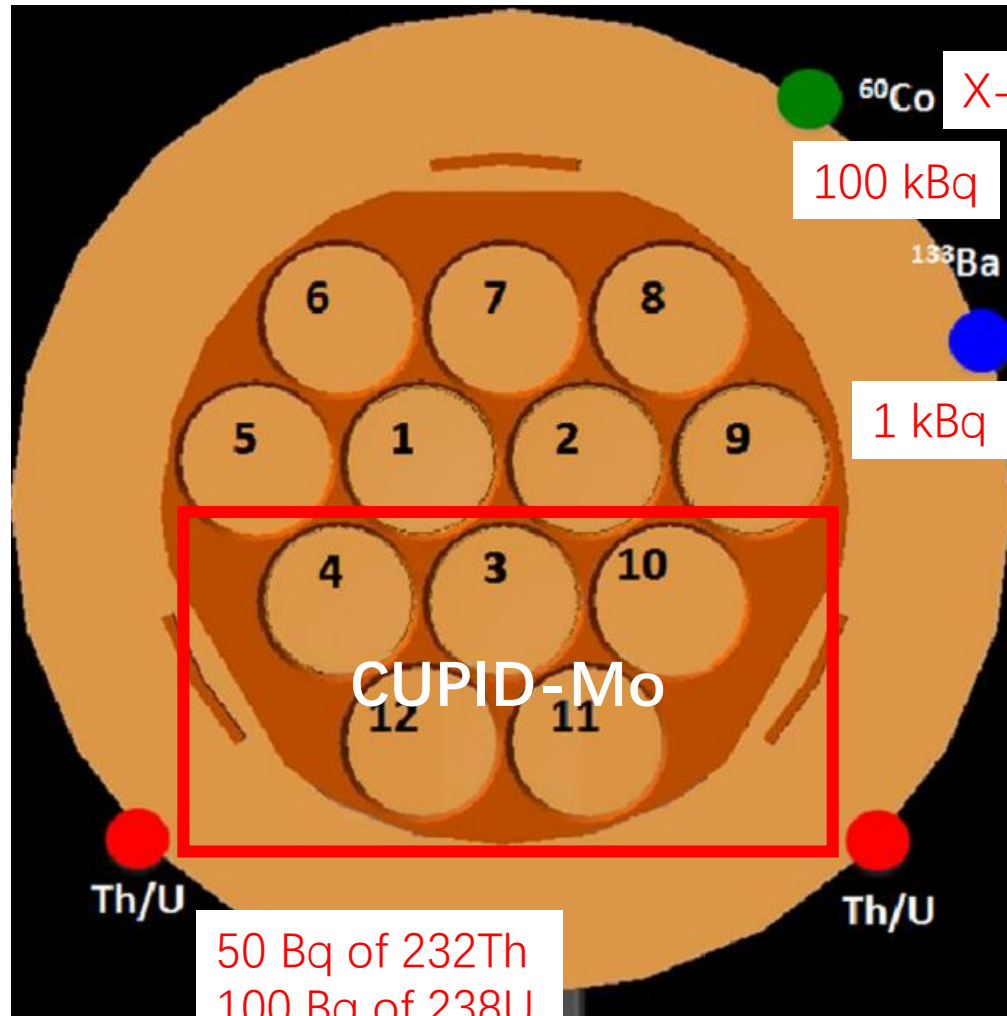


- Wet cryostat, reliquefaction system needed (vibration noise)
- Mechanically decoupled from EDELWEISS-III with three springs<sup>[1]</sup>
- Outer shield: 20 cm lead and 55 cm polyethylene
- Inner shield: 2cm Roman lead & 14cm Roman lead and 10cm polyethylene at 1K-plate
- 98% geometrical coverage muon veto system



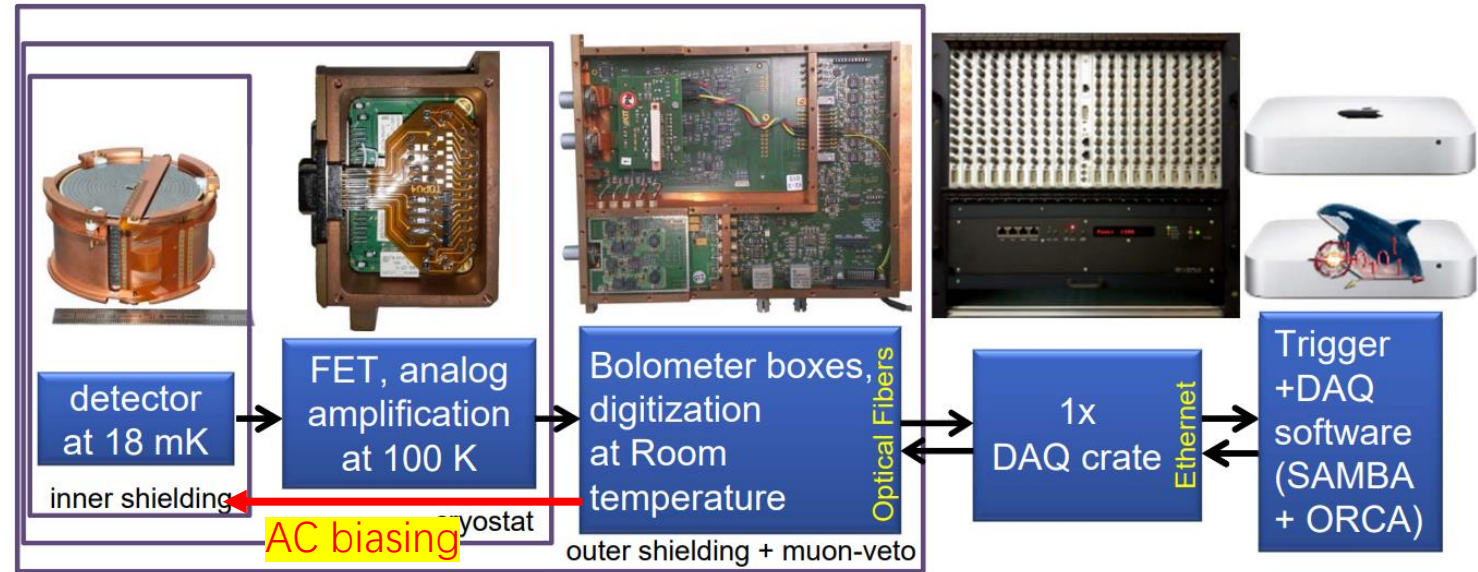
[1] E. Armengaud et al., Eur. Phys. J. C 77, 785 (2017)

# EDELWEISS-III cryogenic



50 Bq of  $^{232}\text{Th}$   
100 Bq of  $^{238}\text{U}$   
Few Bq of  $^{235}\text{U}$

X-ray fluorescence calibration



EDELWEISS-III data path<sup>[2]</sup>

[2] E. Armengaud et al., JINST 12, P08010 (2017)

- 1 LD lost; 2 heaters unable to inject pulses
- NTD @ LDs operate in over-bias regime  $\sim 1\text{M}\Omega$  (but to mitigate the impact of AC biasing)
- Working at 20.7 mK
- Two independent analysis frameworks: DIANA and a CSNSM framework (cross-check)



# LDs performance



- 4.2 ms rise time and 9.2 ms decay time
- Calibration using X-ray fluorescence of Mo & Cu
- First-order polynomial calibration with zero intercepts
- Random trigger events every 101 s to estimate the baseline resolution

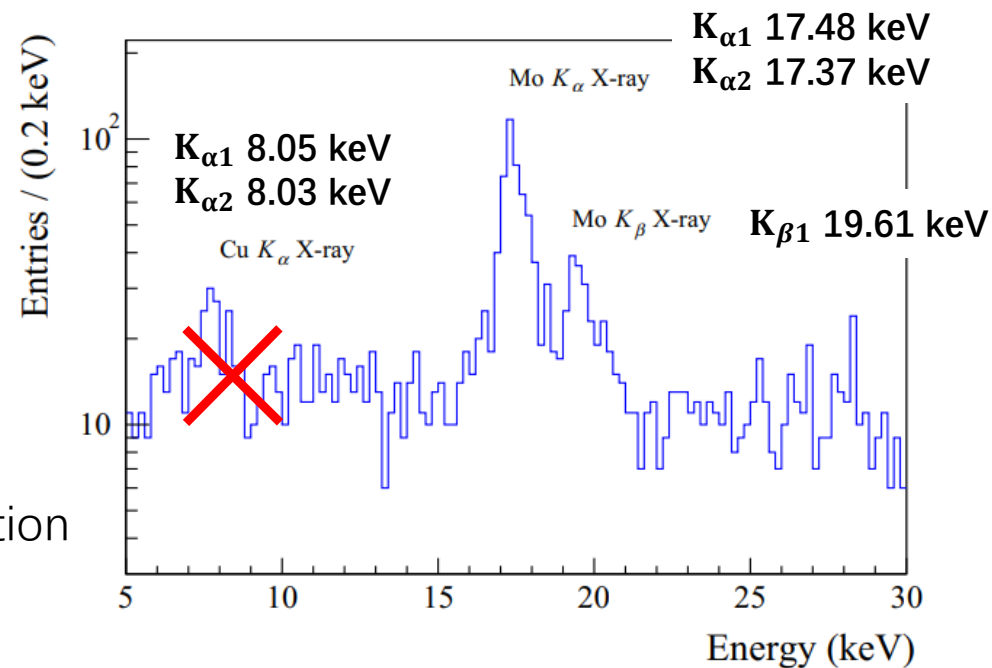
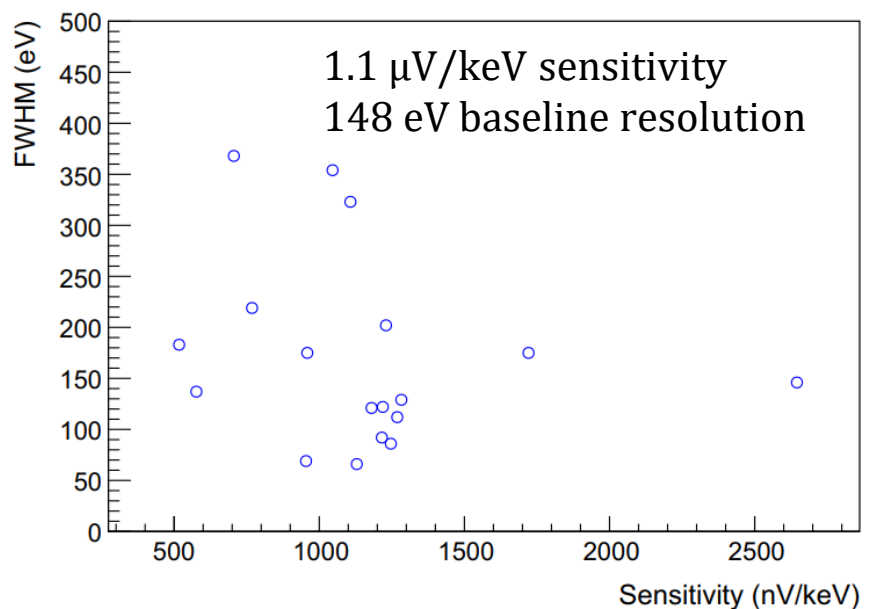


**Fig. 9** Energy spectrum of CUPID-Mo light detector LD2 after a 33 h <sup>60</sup>Co irradiation in the EDELWEISS-III set-up. The Mo  $K_{\alpha}$  X-rays are used for the LD calibration

**Fig. 10** The baseline resolution versus sensitivity for 18/20 Ge LDs operated in the CUPID-Mo experiment at 20.7 mK. One detector is discarded due to having a different NTD (LD 3), while the second is not operational (LD 7, see text)

# LMOs performance



- 24 ms rise time and 299 ms decay time
- Calibration using mixed Th/U source 2.2 days
- neglect nonlinearities & fit using zero and the  $^{208}\text{Tl}$  line
- $^{208}\text{Tl}$  line also used for stabilization

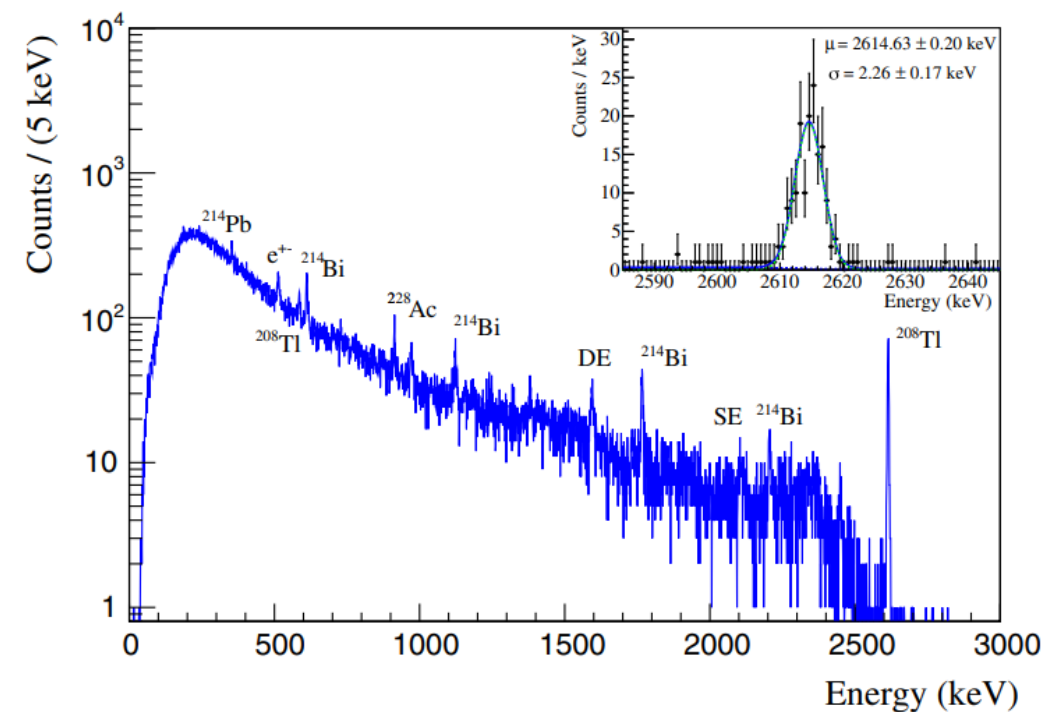
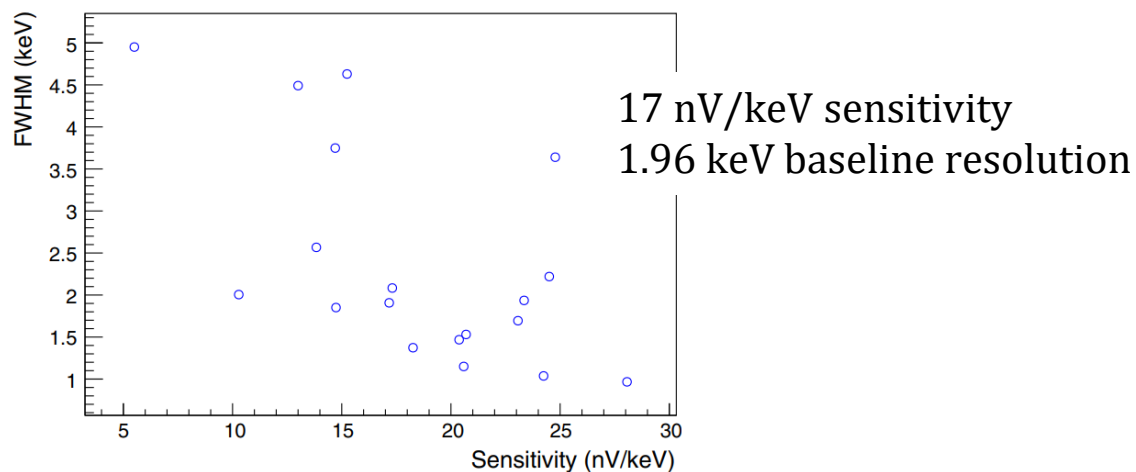
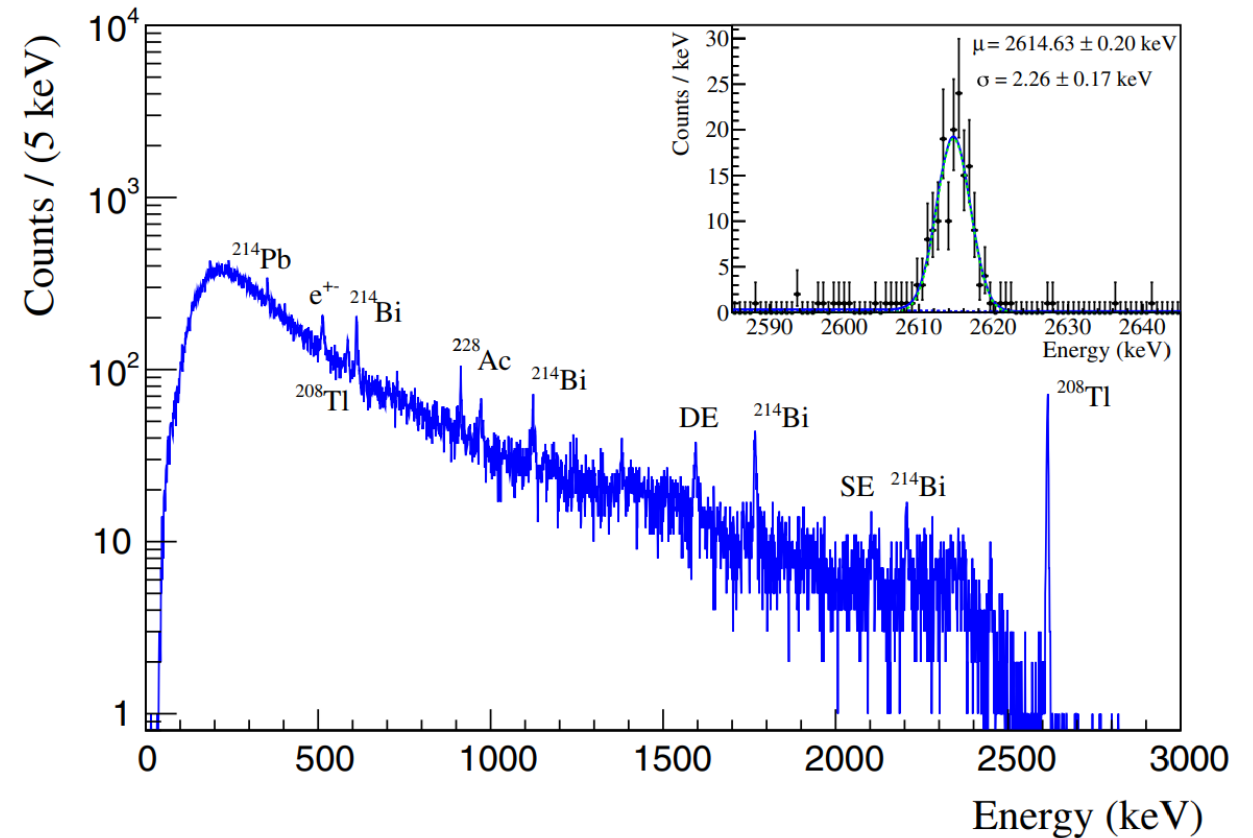


**Fig. 13** Summed calibration spectrum for 19/20  $\text{Li}_2\text{MoO}_4$  bolometers. All the major peaks have been labeled. The inset shows a fit of the  $^{208}\text{Tl}$   $\gamma$  peak at 2614.5 keV

- Cut atypical noise & temperature spikes of the cryostat ~11%
- Pile-up cut in (-1,+2) s window (dominated by heater) ~4%
- baseline slope、rise-time & optimum filter peak position within 5 median absolute deviations (MAD)
- Relative Light Yield within  $4\sigma$  of the mean amplitude



- Single LD with higher RLY
- RLY difference between top and bottom LDs is a result of the support structure design.
- Summed light collection  $\sim 1.35$  keV/MeV
- Use the bottom LDs for further analysis

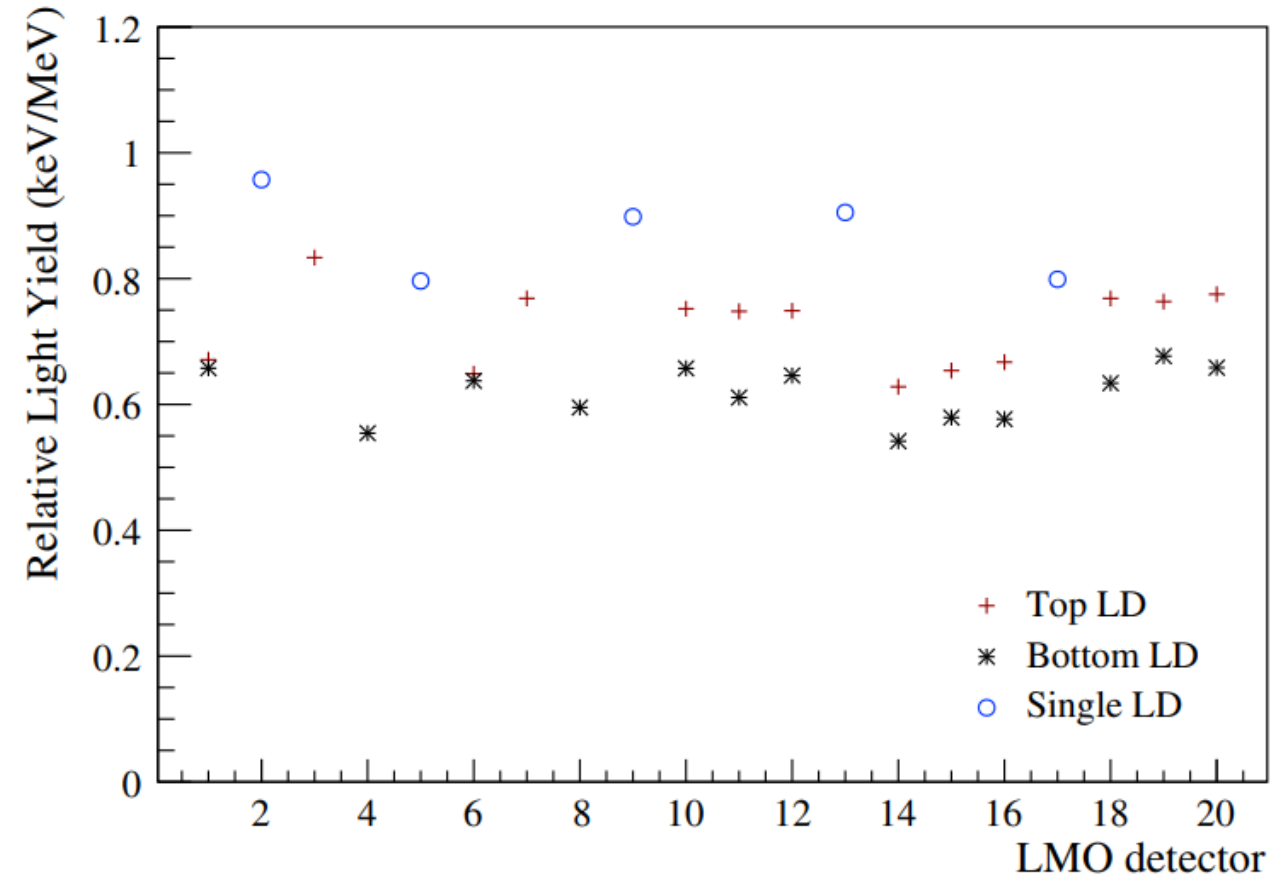
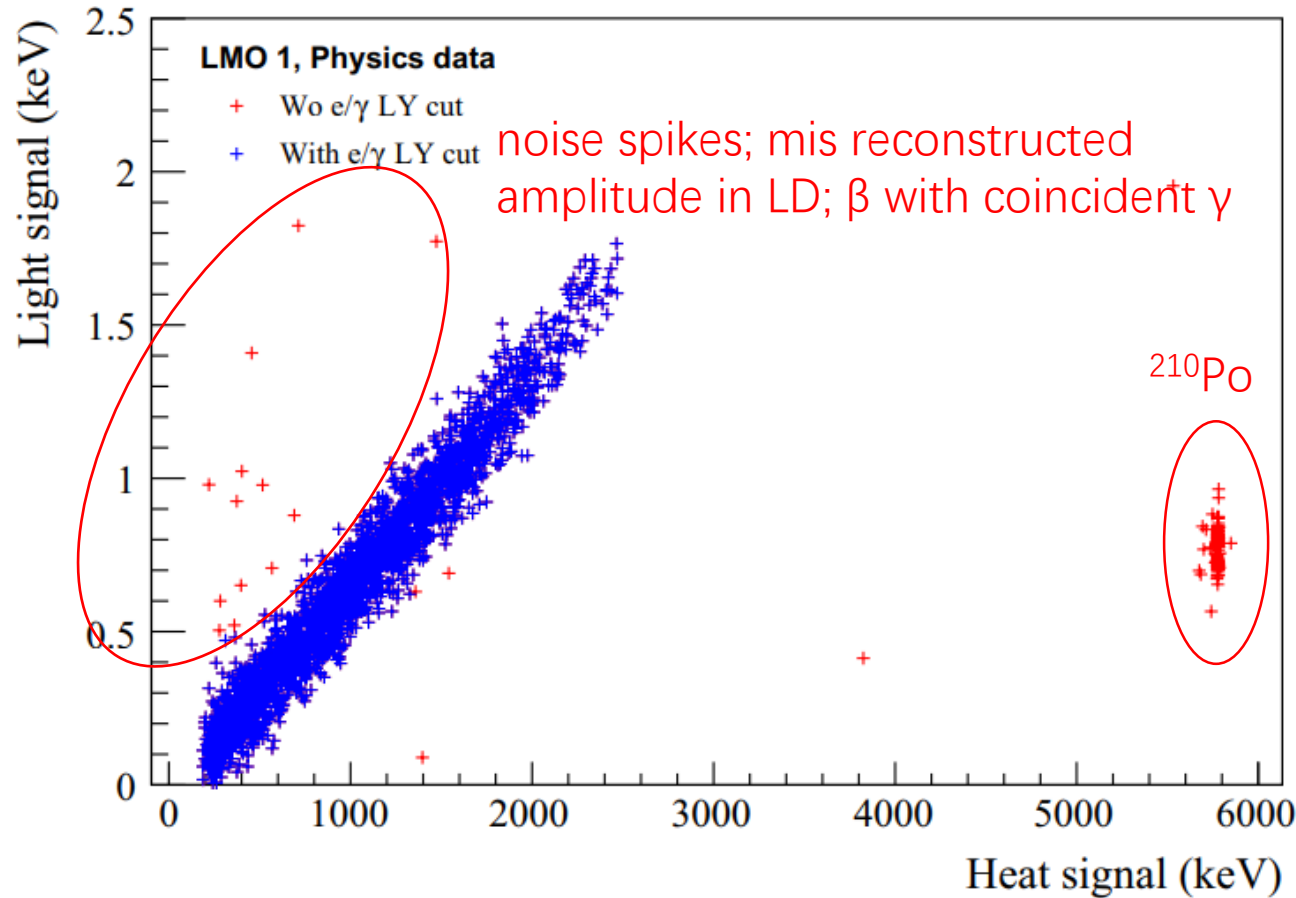


**Fig. 14** Relative Light Yields for all of the  $\text{Li}_2^{100}\text{MoO}_4$  crystals. The differences in RLY trace the expected light collection efficiencies due to the design of the towers, see Sects. 2.5 and 2.6



light quenching of  $\alpha$  particles with respect to  $\gamma$  /  $\beta$  particles of  $(19.7 \pm 1.0)\%$

$$DP = \frac{\mu_{\gamma} - \mu_{\alpha}}{\sqrt{\sigma_{\gamma}^2 + \sigma_{\alpha}^2}}$$

The resulting median discrimination power is  $15.0$ , with the worst performing detector having a discrimination power of 6

**Fig. 15** Light yield versus heat signal scatter-plot using 11 days of physics data from LMO 1. The presented detector has the highest  $^{210}\text{Po}$  contamination to illustrate best the distributions of  $\alpha$  and  $\gamma$  events and the scintillation light quenching for  $\alpha$  events

Additional cut:  
100 ms M1 cut to reject multi-Compton and muon shower

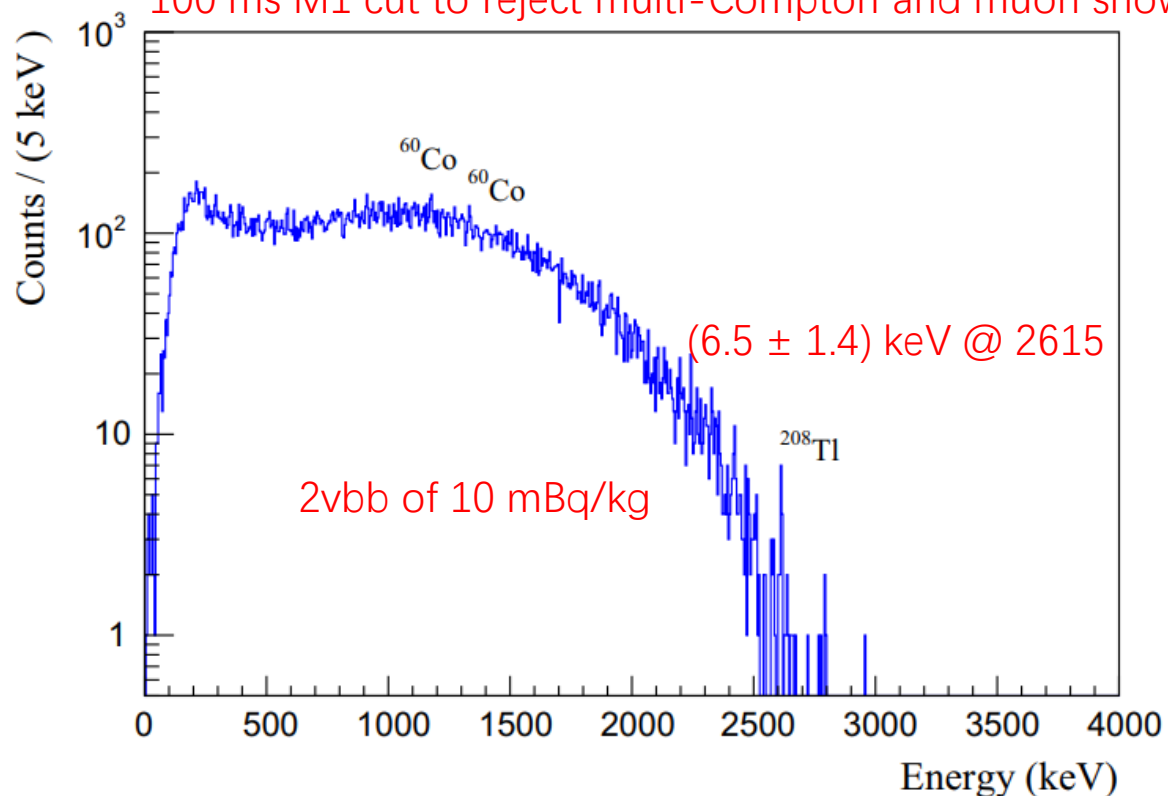


**Fig. 16** Summed background spectrum using 11.1 days of data from 19/20  $\text{Li}_2^{100}\text{MoO}_4$  cryogenic detectors of the CUPID-Mo experiment

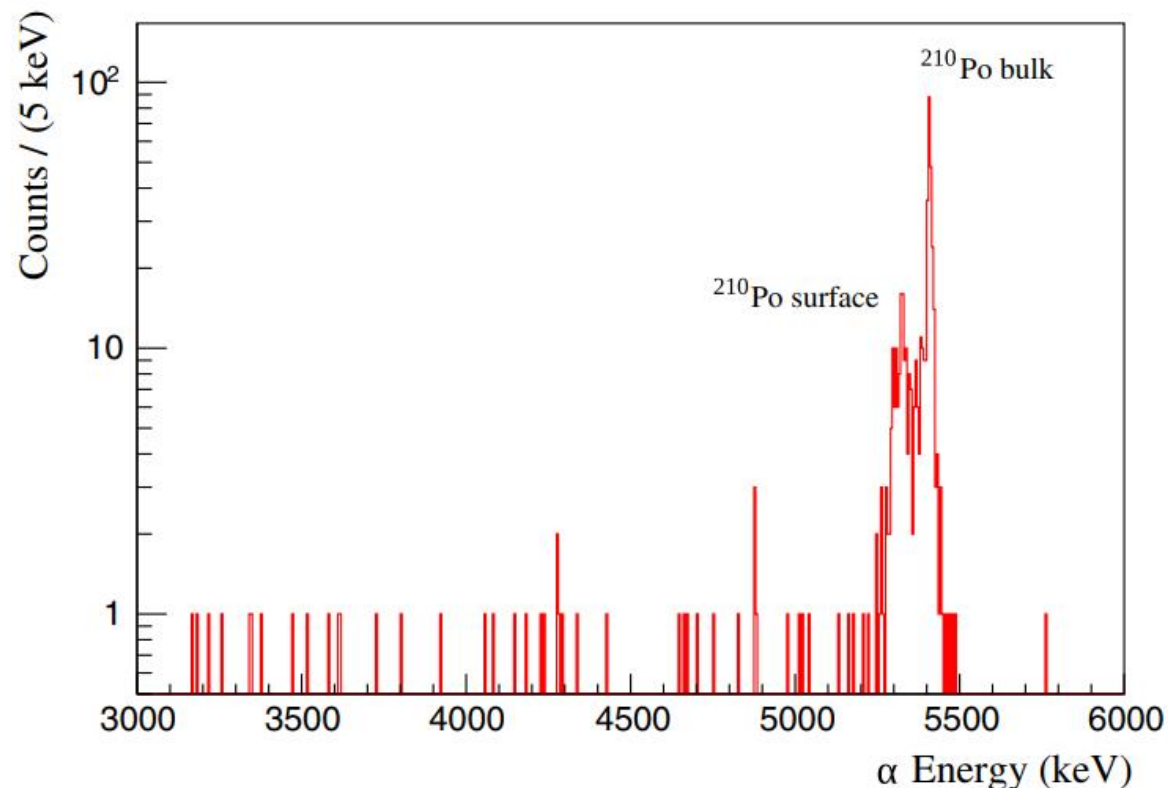
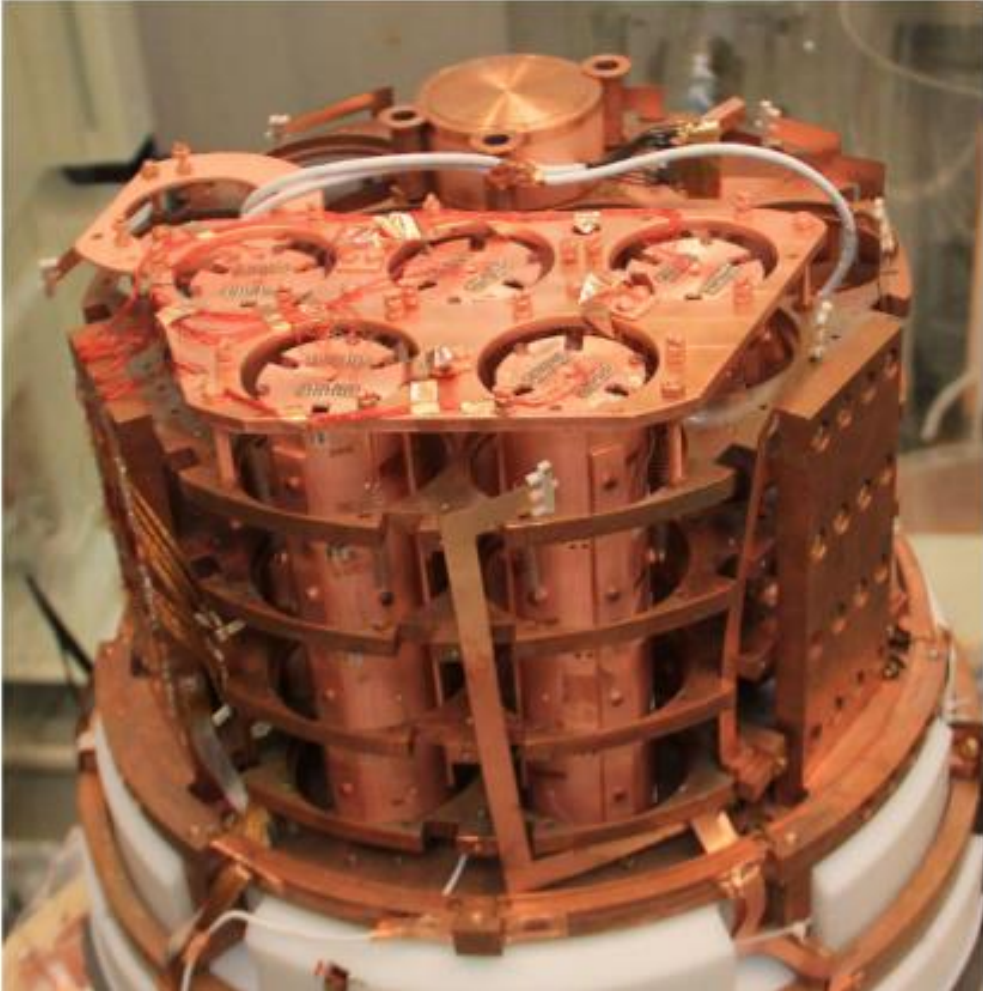


**Fig. 17** Summed alpha region using 19/20 detectors. No RLY cut applied. (For details see text.)

Number of events in a  $\pm 30$  keV window around each nominal decay energy is compatible with zero at the  $2\sigma$  level for all of the U Th chain signatures.

Conservative upper limit  $2\mu\text{Bq/kg}$  (Th-series) and  $3\mu\text{Bq/kg}$  (U-series) (90% CL) using the largest observed event count



- @ Modane underground laboratory
- 20 enriched LMO (97%), 0.2 kg each ( $\Phi 44 \times 45$  mm), 20 LD
- 20.7 mK working temperature
- 5.3 keV (6.5 keV) FWHM at 2615 keV, in calibration (physics) data
- light yield for  $\gamma$  / $\beta$  events (0.6–0.9 keV/MeV)
- $\alpha$  rejection efficiency  $> 99.9\%$  (discrimination power  $\sim 15$ )
- Crystals' radiopurity:  $\leq 3 \mu\text{Bq/kg}$  of  $^{226}\text{Ra}$  and  $\leq 2 \mu\text{Bq/kg}$  of  $^{232}\text{Th}$

Thanks